Shahrood University of Technology

Iranian Society of Mining Engineering (IRSME)

THOMSON REUTERS

Numerical Stability Analysis of Undercut Slopes Evaluated by Response Surface Methodology

Hassan Sarfaraz[1], Mohammad Hossein Khosravi[1*], and Thirapong Pipatpongsa[2]

1. School of Mining Engineering, College of Engineering, University of Tehran, Tehran, Iran
2. Department of Urban Management, Kyoto University, Kyoto, Japan

Article Info	Abstract
	One of the most important tasks in designing the undercut slopes is to determine the maximum stable undercut span to which various parameters such as the shear strength of the soil and the geometrical properties of the slope are related. Based on the arching phenomenon, by undercutting a slope, the weight load of the slope is transferred to the adjacent parts, leading to an increase in the stability of the slope. However, it may also lead to a ploughing failure on the adjacent parts. The application of counterweight on the adjacent parts of an undercut slope is a useful technique to prevent the ploughing failure. In other words, the slopes become stronger as an additional weight is put to the legs; hence, the excavated area can be increased to a wider span before the failure of the slope. This technique could be applied in order to stabilize the temporary slopes. In this work, determination of the maximum width of an undercut span is evaluated under both the static and pseudo-static conditions using numerical analyses. A series of tests are conducted with 120 numerical models using various values for the slope angles, the pseudo-static seismic loads, and the counterweight widths. The numerical results obtained are examined with a statistical method using the response surface methodology. An analysis of variance is carried out in order to investigate the influence of each input variable on the response parameter, and a new equation is derived for computation of the maximum stable undercut span in terms of the input parameters.

1. Introduction

In open-pit mining, stabilizing the mine pit in order to avoid any occurrence of slope failure is the most vital issue, especially during the mining operations. Advancement of the blasting and excavation technologies as well as the increased capacity of loading and hauling machines have caused a higher percentage of ore to be exploited. Consequently, the geometry of mine pits has become deeper and steeper. Along with these advancements, geotechnical engineering should provide appropriate solutions to the mine excavation problems. The arching effect is an important phenomenon in rock and soil media. In general, arching happens when the rigidity of two adjacent regions is different due to a disturbance in the initial distribution of stress. In this situation, the redistribution of stress takes place such that more stress is applied to the region with a higher rigidity, and less stress is applied to the region with a lower rigidity [1]. The formation of arching in the hoppers of granular materials has first been studied by Janssen [2]. He concluded that the horizontal pressure applied to the hopper wall would not increase linearly with depth. However, increments in pressure would decrease with depth until the pressure reached a constant value at a specified depth. Janssen [2] has established the theory of arching based on this investigation. Terzaghi [3] has studied the formation of arching in geotechnical materials. After the introduction of arching in granular soil by Terzaghi, the researches tried to investigate this phenomenon in different

✉ *Corresponding author: mh.khosravi@ut.ac.ir (M.H. Khosravi).*

geotechnical structures such as retaining walls, tunnels, and slopes. The stability of slopes is a major problem in geotechnical engineering as slope failure hazards may cause catastrophic damage and human casualties. Wang and Yen [4] were the first to investigate the soil arching effects in slopes. Later, Bosscher, and Gray [5] have studied the arching effect in sandy slopes through the use of physical models.

In surface mining and this work, the term "undercut slope" refers to those slopes where the excavation operations are carried out in their front part. Determining the optimum size of the undercut span is an important problem. In other words, its maximum size depends on the strength properties of the slope materials, and its minimum size depends on the desired capacity of production and the size of the mining equipment [6]. Many researchers have investigated the stability of slopes, and different techniques including anchorage and geogrid have been developed for stabilizing slopes [7, 8]. Also there are studies on the effect of non-persistent joints on the sliding direction of rock slopes [9, 10]. Sun *et al*. [11] have presented a design approach to stabilize slopes with piles. Other researchers performed examinations of studies on this subject [12-14]. Using the limit equilibrium method, Ausilio *et al*. [15] have presented an analytical solution for stabilizing slopes with piles. Kourkoulis *et al*. [16, 17] have presented a hybrid method for analyzing and designing slope stabilization using one row of piles. Pipatpongsa *et al*. [18] have proposed a technique for excavation based on the arching effect and the cut and fill method in the Mae-Moh open-pit mine. This method increases the slope stability without using any support equipment. The formation of the arching effect in undercut slopes was investigated by the 1g physical modelling [19] and the centrifugal modelling [20]. The results obtained from pressure sensors and the image processing technique showed that during the undercutting process, a fraction of yielded soil weight was transmitted to the adjacent rigid areas, which depended on the strength properties of those regions. It was concluded that the arching phenomenon in undercut slopes was independent from the scale. Khosravi *et al*. [21] have introduced the application of counterweight balance for

stabilizing undercut slopes. Sarfaraz *et al*. [22] have evaluated the stability analysis of undercut slopes using the artificial neural network.

A pseudo-static slope stability analysis is a simple method for considering the dynamic loads applied to a slope by assuming additional static loads. The first application of this method is attributed to Terzaghi [23]. The main purpose of this paper is to present a relationship for computing the maximum width of the undercut span as a function of the slope angle, the horizontal seismic acceleration coefficient (K_h), and the width of the counterweight (Cw) for the static and pseudo-static conditions. In this way, a series of 120 numerical simulations are performed using the FLAC3D software. At first, for validation of the numerical modelling, the numerical results obtained were compared with the corresponding experimental test results, and next, the response surface methodology (RSM) was used to interpret the numerical simulations. Then the results obtained were discussed.

2. Numerical modelling

A series of numerical models have been established by Khosravi *et al*. [24], as schematically illustrated in Figure 1. As their study was limited to a constant slope angle of 50 degrees under the static conditions, the modelling for various slope angles as well as the pseudo-static conditions was required to be developed.

In this work, FLAC3D, as a finite difference software, was used for modelling the continuum media. This software is based on the Lagrangian formulation, which makes it suitable for large deformation analyses [25]. A schematic representation of the numerical model is shown in Figure 2. The geometry of the numerical model is the same as the physical model conducted by Khosravi *et al*. [21]. As indicated in this figure, the model consists of cubic elements with a size of 2 cm. The model is composed of two parts: the base part with the dimensions of W = 100 cm and L_T = 40 cm and the slope part with the dimensions of W = 100 cm and L_S = 60 cm. The thickness of the model is H = 6 cm in both the base and slope parts. In this figure, Cw stands for the width of the counterweight.
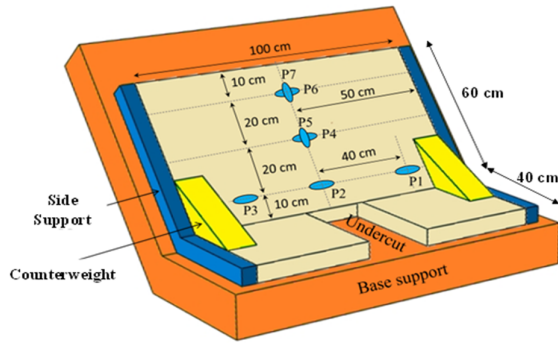
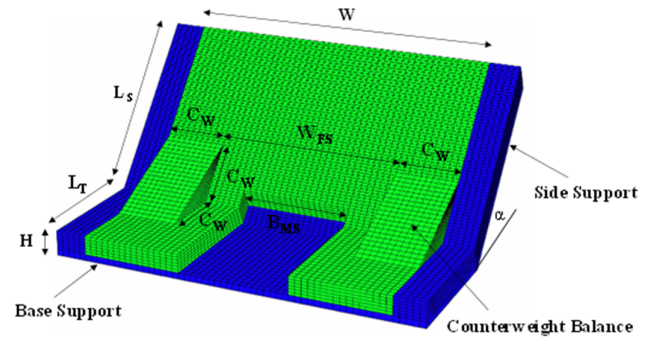**Figure 1. Schematic representation of the physical model [24].**

Figure 2. Schematic representation of the numerical model.

The constitutive criteria of Mohr-Coulomb and linear elasticity are used for the soil, and the base and side supports, respectively. The mechanical properties of the soil (silica sand No. 6) are presented in Table 1. The material is assumed to be isotropic and homogeneous. For a boundary condition, the base and side supports are considered in rigid and fixed in all directions.

The forces in the model are allowed to balance after the preparation and before the undercut process. When the maximum unbalanced force in the model is reduced to zero (i.e. 1e-5), (as shown in Figure 3), the model is ready for undercutting.

Table 1. Material properties of silica sand No. 6 [24].

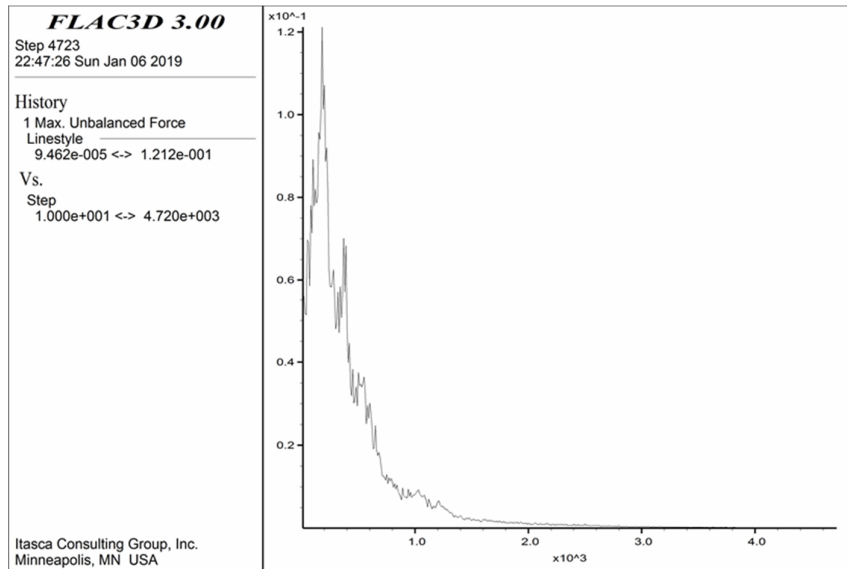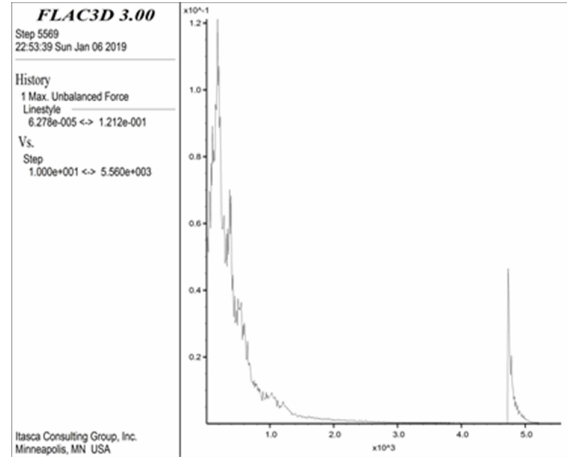|	
Density	1395 kg/m^3
Elastic modulus	4 MPa
Poisson's ratio	0.25
Tensile strength	0 Pa
Normal interface stiffness	1 GPa/m
Shear interface stiffness	1 GPa/m
Internal friction angle	41.5˚
Interface friction angle	18.5˚
Cohesion of soil	0.8 kPa
Interface cohesion	0.1 kPa

Figure 3. Change in maximum unbalanced force before the undercut process.

For each slope angle, the front central part is excavated in the subsequent steps with a width of 4 cm (Figure 4 (a)). In each step of the excavation, the width of the undercut span is increased by 2 cm leftward and 2 cm rightward. After each step, the numerical code is run, and the unbalanced force is computed. When this force approaches zero, the numerical model reaches a stable condition (Figure 4 (b)), and the next step of the excavation is performed. If the unbalanced force does not approach zero, the slope is considered to be in an unstable condition, and the maximum width of the undercut span (B_f) is reached.
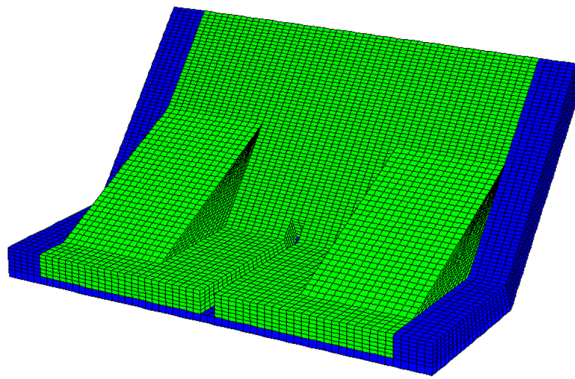
(a) Geometry of the model (undercut span: 4 cm)   **(b) Plot of the unbalanced force**

Figure 4. Initial step of the excavation process in α = 50°, Kh = 0, and Cw = 30 cm.

The variation in the unbalanced force with a slope of 50°, $K_h = 0$, and Cw = 30 cm is shown in Figure 5. According to this figure, after each step of the excavation in front of the slope, an unbalanced force develops and then decreases until it approaches zero. As shown in Figure 5, in the 1th to 8th steps for undercut processing, the unbalance force is reduced to 1e-5 in less than 100000 solving cycles. However, in the 9th step of an undercut, it reaches 1e-5 in most solving cycles, while in the 10th step, the unbalanced force does not reach zero. In other words, with increase in the solving cycles, the value of this force is increased; therefore, the slope is considered to be in an unstable condition, and sliding occurs.
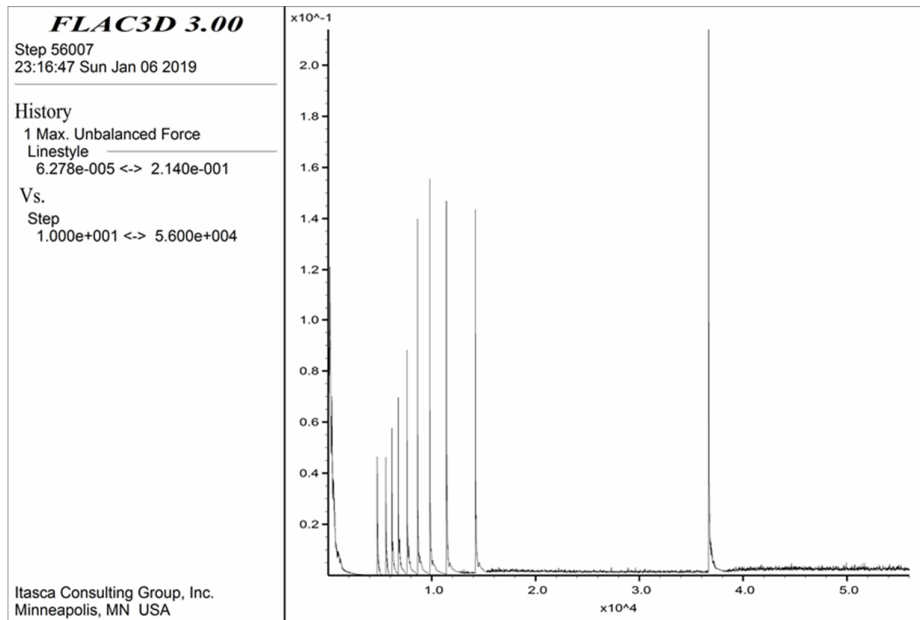

Figure 5. Final step of the excavation process in α = 50°, Kh = 0, and Cw = 30 cm.

In the numerical model with α = 50°, $K_h = 0$, and C_w = 0, 20, and 30 cm, the contours of the failure modes are as presented in Figure 6 (a)-(c). The initiation of shear cracks was observed from the corner of the undercut region, and most of the other areas were under tension. In this figure, the symbols *p* and *n* indicate the state of the model in the previous and the current steps, respectively.
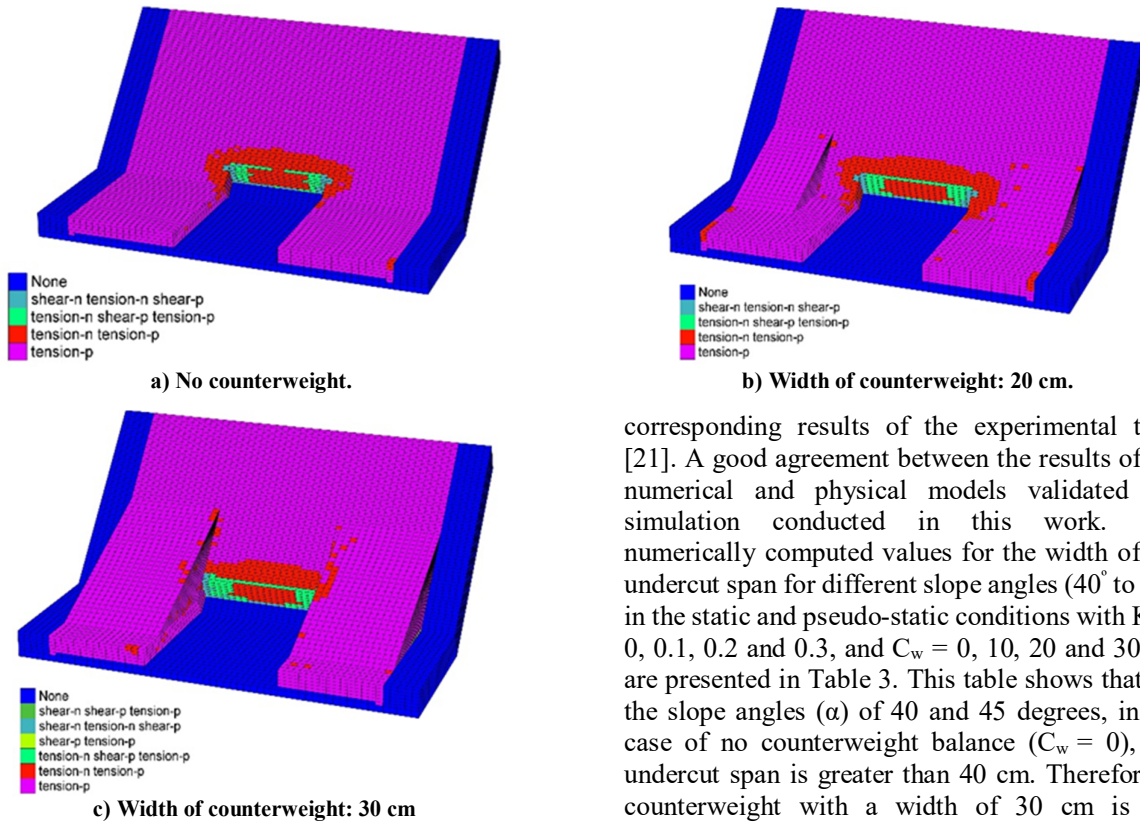
a) No counterweight.

b) Width of counterweight: 20 cm.

c) Width of counterweight: 30 cm

Figure 6. Crack initiation observed in the numerical model with α = 50° and K_h = 0.

At first, in Table 2, the numerical results under the static conditions (K_h = 0) are compared with the corresponding results of the experimental tests [21]. A good agreement between the results of the numerical and physical models validated the simulation conducted in this work. The numerically computed values for the width of the undercut span for different slope angles (40° to 75°) in the static and pseudo-static conditions with K_h = 0, 0.1, 0.2 and 0.3, and C_w = 0, 10, 20 and 30 cm are presented in Table 3. This table shows that for the slope angles (α) of 40 and 45 degrees, in the case of no counterweight balance (C_w = 0), the undercut span is greater than 40 cm. Therefore, a counterweight with a width of 30 cm is not applicable. The effect of the counterweight on the slope angle under the static condition is shown in Figure 7. In this figure, it is clear that the counterweight has no supporting influence on the slopes steeper than 60°.

Table 2. Comparison of the numerical and physical results under the static condition (Kh = 0).

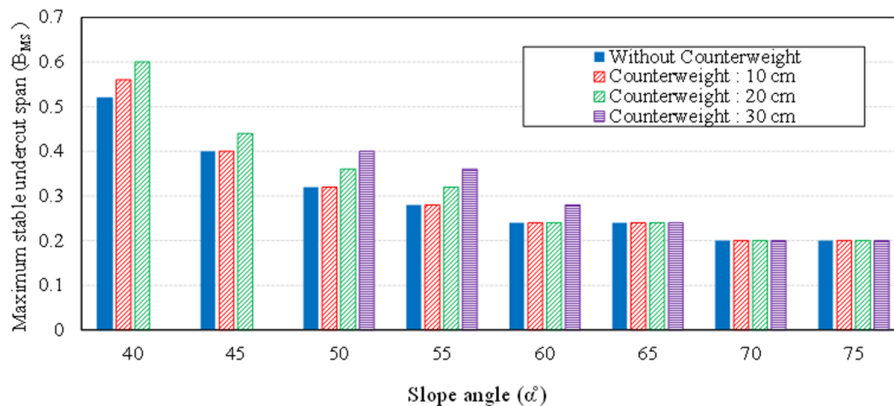| Angle of slope (α: degree)	Width of counterweight (C_w: cm)	Maximum stable undercut span (B_{MS}: cm)	
		Physical models [21]	Physical models [21]
40	0	50	52
50	0	35	32
	20	40	36
	30	45	40
60	0	25	24
70	0	20	20

Figure 7. Effect of counterweight on slope angle under the static condition (Kh = 0).

Table 2. Results of the numerical model in terms of undercut span (B$_{MS}$: cm).

Angle of slope (α: degree)	Width of counterweight (C_w: cm)	K_h			
		0	0.1	0.2	0.3
40	0	52	36	0.2	24
	10	56	36	28	24
	20	60	36	28	28
45	0	40	32	32	24
	10	40	32	28	24
	20	44	32	28	24
50	0	32	28	28	24
	10	32	28	24	24
	20	36	28	24	24
	30	40	32	24	24
55	0	28	24	28	20
	10	28	24	24	20
	20	32	24	24	20
	30	36	28	24	24
60	0	24	24	24	20
	10	24	24	20	20
	20	24	24	20	20
	30	28	28	20	24
65	0	24	20	24	20
	10	24	20	20	20
	20	24	20	20	20
	30	24	24	20	20
70	0	20	20	20	16
	10	20	20	20	16
	20	20	20	20	16
	30	20	20	20	20
75	0	20	20	20	4
	10	20	20	16	4
	20	20	20	16	4
	30	20	20	16	4

The maximum normalized stable undercut span (B$_{MS}$/W$_{FS}$) in terms of the normalized free span (W$_{FS}$/W) is illustrated in Figure 8, where $W = 2C_W + W_{FS}$; the free span is denoted as W$_{FS}$ (Figure 2). Figure 8 demonstrates that for all slope angles, the undercut span increases by the decrease in the free span. In other words, increasing the counterweight leads to a rise in the undercut span. Thus this work confirms the results of Khosravi *et al*. [21], namely, that applying a counterweight is a beneficial technique for stabilizing the undercut slopes. However, it is noticeable that the effect of the counterweight on slopes dipping more than 60° is ignorable.

3. Response Surface Methodology (RSM)

RSM is an appropriate method for the optimization process [26]. In this technique, the particular relationship between the response and the independent input variables is unclear. Hence, the first step is to find the appropriate approximation for the correct functional relationship between the output and the independent input variables [26]. In order to describe the problem, a polynomial or a linear function is used. When a non-linear relationship exists in the system, the linear model loses its proficiency. Therefore, the quadratic model suggested by Montgomery [27] was chosen in this work.

$$y = \alpha_0 + \sum_{i=1}^{m} \alpha_i x_i + \sum_{i=1}^{m} \alpha_{ii} x_i^2 + \sum\sum \alpha_{ij} x_i x_j + \varepsilon \quad (1)$$

where:

y: Response;

m: Number of variables;

α_0 : Constant term;

α_i : Coefficients of the linear term;

α_{ii} : Coefficients of the quadratic term;

α_{ij} : Coefficients of the interaction term;

x_i : Variable;

ε: Residual associated with the experimental data.

The quadratic equation is used in RSM in order to establish the equations between three input variables and one response. The independent input variables (Dip, W_{FS}/W, K_h) are given in Table 3, and the response (B_{MS}/W_{FS}) of the RSM analysis is given in Table 5.
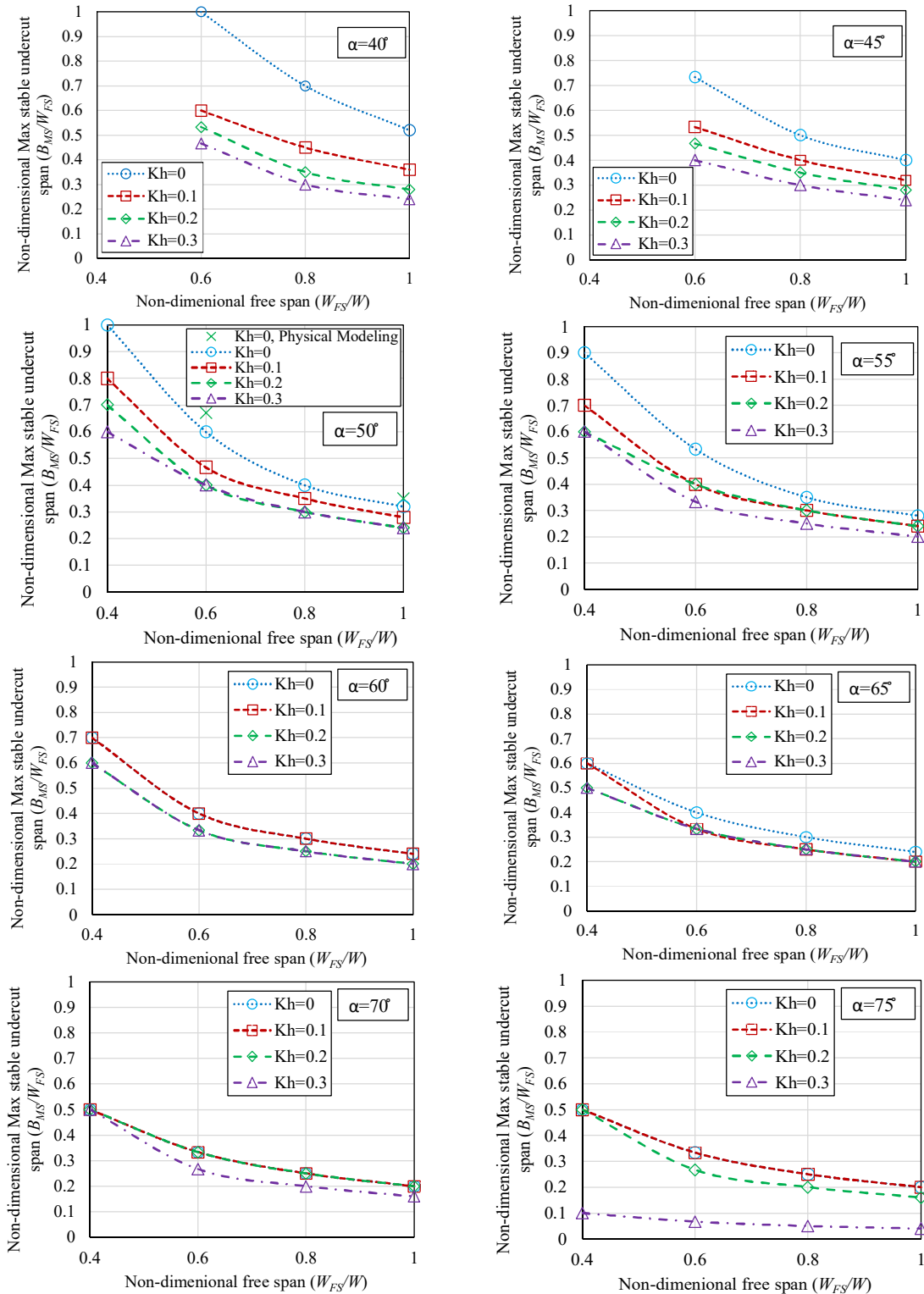

Figure 8. Numerical results revealing maximum undercut span *vs.* free span.

Table 3. Independent input variables.

Factor	Variable	Minimum	Maximum	Mean	Std. Dev.
A	Dip	40°	75°	58.5°	11.1634
B	W_{FS}/W	0.4	1	0.72	0.2175
C	K_h	0	0.3	0.15	0.1123

Table 4. Response of RSM analysis.

Response	Parameter	Analysis	Model	Minimum	Maximum	Mean	Std. Dev.	Ratio
R1	B_{MS}/W_{FS}	Polynomial	Quadratic	0.04	1.00	0.38	0.18	25

3.1. Analysis of Variance (ANOVA)

ANOVA is a technique used to evaluate the dependability of a model. Without ANOVA, the mathematical equations for the data obtained by RSM may not effectively explain the considered experiment. The importance of regression is assessed by the ratio between the mean of the square regression and the mean squares of the residuals, according to their degrees of freedom. Higher values for the F-value ratio indicate that the statistical model is appropriately fitted to the experimental data [28]. The proposed model for the maximum normalized undercut span (B_{MS}/W_{FS}) is presented in Table 6. Also the quadratic model is selected as the best model for the fitting data.

Table 6. Statistical parameters of the presented model for the response.

Model	R-squared	Adjusted R-squared	Predicted R-squared	F-value
Quadratic	0.9044	0.8984	0.8813	151.28

With higher F-values, the significance of the proposed model becomes better. For the maximum normalized undercut span, an F-value equal to 151.28 is suggested for the validation of the quadratic model. The assessment of the fitted model is usually determined by the correlation parameter. According to the values presented in Table 5, the proposed model has a good correlation coefficient. Besides, the adjusted R-squared coefficient is notably different from the predicted R-squared coefficient. A plot of the actual versus the predicted values is shown in Figure 9(a). The relationship between the normal probability and the studentized residues is presented in Figure 9(b).
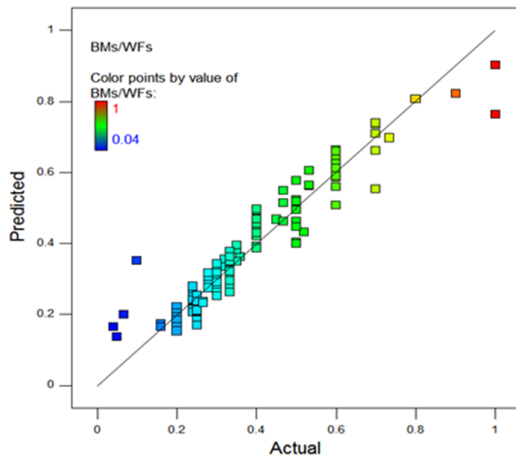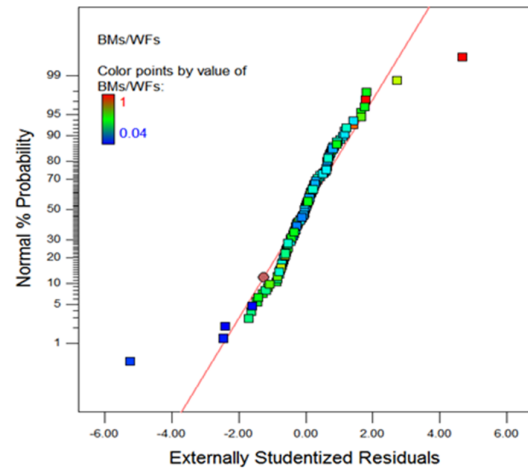

a). Predicted values versus actual values.   **b). Normal probability versus studentized residuals.**

Figure 9. ANOVA for B_{MS}/W_{FS}.

Figure 9(b) is used to check the normalization of the residual values. If the residual points are along the straight line, the normal probability plot shows that the residual values are distributed normally. The model is said to have a higher validity as the shape of the normal probability plot becomes more linear. The results of the variance analysis are presented in Table 7. The effective variables, sum of the squares, number of degrees of freedom (number of effective variables), mean square, and F and P values are shown in this table.

Table 7. Results of variance analysis for BMS/WFS.

Source	Sum of squared	df	Mean squared	F-value	p-value prob > F	Significance
Model	3.61	7	0.52	151.28	< 0.0001	✓
A: Dip	1.10	1	1.10	321.24	< 0.0001	
B: W_{FS}/W	2.41	1	2.41	708.13	< 0.0001	
C: K_h	0.50	1	0.50	147.48	< 0.0001	
AB	0.12	1	0.12	36.28	< 0.0001	
AC	0.071	1	0.071	20.88	< 0.0001	
BC	0.044	1	0.044	12.91	0.0005	
B^2	0.23	1	0.23	67.19	< 0.0001	

As shown in Table 7, values of "P-value prob > F" less than 0.05 illustrate that the model terms are significant and values greater than 0.1 indicate that the model terms are insignificant. Therefore, the variables A, B, C, AB, AC, BC, and B^2 are significant. The final equation in terms of the influential variables is presented as follows:

$$\left(\frac{B_{MS}}{W_{FS}}\right) = 2.82585 - 0.022121(Dip)$$
$$-3.2179\left(\frac{W_{FS}}{W}\right) - 2.2801(K_h)$$
$$+0.01452\left(Dip \times \frac{W_{FS}}{W}\right) + 0.019775(Dip \times K_h) \qquad (2)$$
$$+0.7979\left(\frac{W_{FS}}{W} \times K_h\right) + 1.1272\left(\frac{W_{FS}}{W}\right)^2$$

3.2. Response surface analysis of maximum undercut span

The influence of the input parameters, both individual and simultaneous, on the response is illustrated in Figures 10 to 12. In these figures, in order to determine the effect of each variable on the response (B_{MS}/W_{FS}), the other input variables are kept constant at their mean values. As shown in Figure 10(a), as the dip angle increases, the maximum normalized undercut span decreases significantly. According to Figure 10(b), by increasing the normalized free span (W_{FS}/W), the maximum normalized undercut span decreases non-linearly. As it can be seen in Figure 10(c), the maximum normalized undercut span decreases slightly when the horizontal acceleration coefficient increases from zero (static condition) to 0.3.

In Figure 11, the interaction effect is shown in a 2D plane. According to Figure 11(a), the simultaneous increase in both the dip angle and the normalized free span variables results in a reduction in the maximum normalized undercut span. However, the dip angle variable has more of an influence on the maximum normalized undercut span than the normalized free span variable. As it can be seen in Figure 11(a)-(c), the dip angle and the horizontal acceleration coefficient have maximum and minimum influences, respectively, on the decrease in the maximum normalized undercut span.

In Figure 12, the interaction effect is shown in a 3D space. According to Figure 12(a), the effect of the counterweight width on a mild slope is greater than that on a steep slope. In steep slopes, the counterweight does not have a significant influence on the stability of the undercut slopes. As indicated in Figure 12(b), for steep slopes, the maximum width of undercut slopes does not change under either the static or the pseudo-static conditions. In the static conditions, by increasing the angle of the slope, the maximum width of the undercut span will decrease sharply. Also as the horizontal acceleration coefficient increases, the maximum width of the undercut span decreases at a low rate. According to Figure 12(c), for a constant value of the normalized free span, the maximum normalized undercut span decreases as the horizontal acceleration coefficient increases from 0 to 0.3. However, the rate of decrease in the maximum normalized undercut span is greater with lower values for the normalized free span.
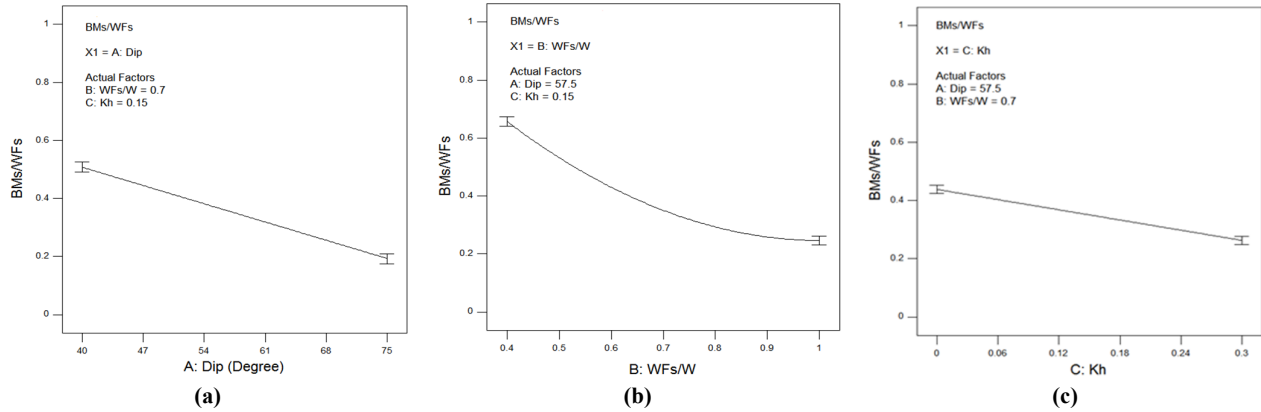
Figure 10. Effects of the dip angle (a), normalized free span (b) and horizontal acceleration coefficient (c) on the maximum normalized undercut span.
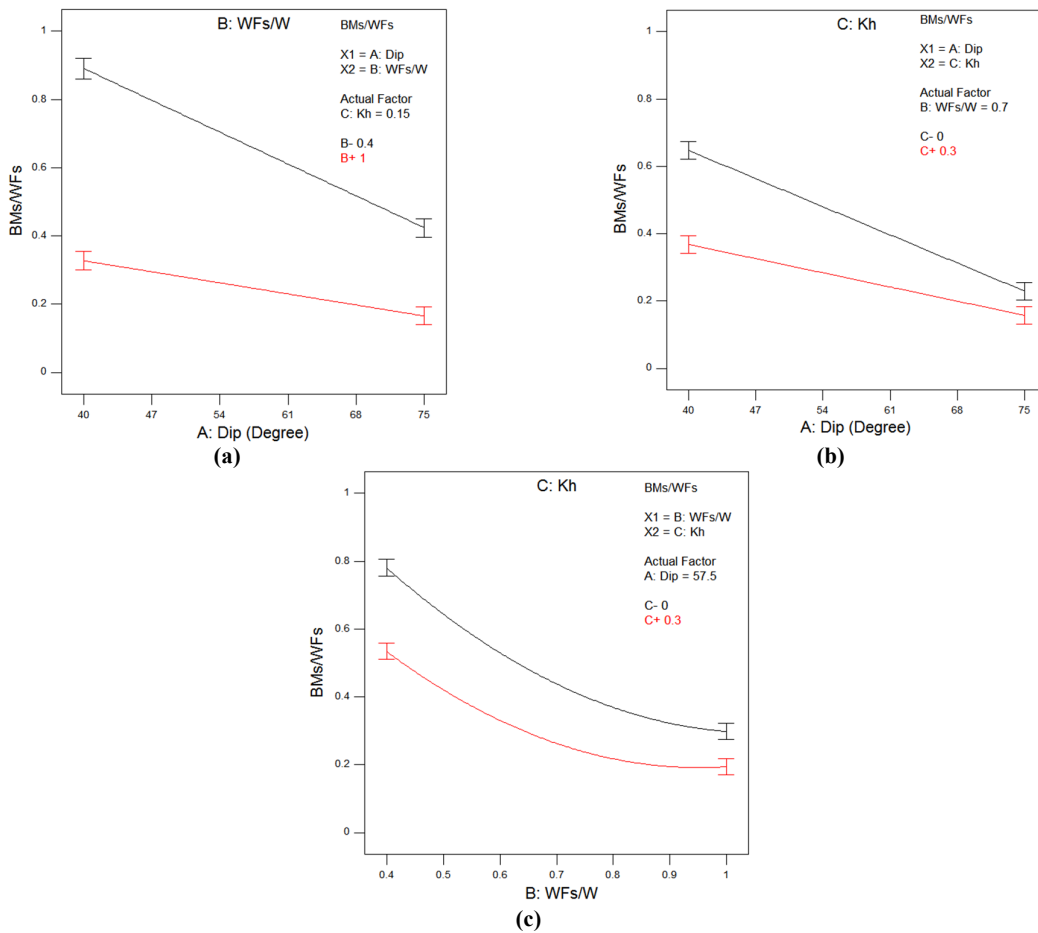

Figure 11. Effects of the dip angle and normalized free span interaction (a), dip angle and horizontal acceleration coefficient interaction (b), normalized free span and horizontal acceleration coefficient interaction (c) in the 2D plane on the maximum undercut span.
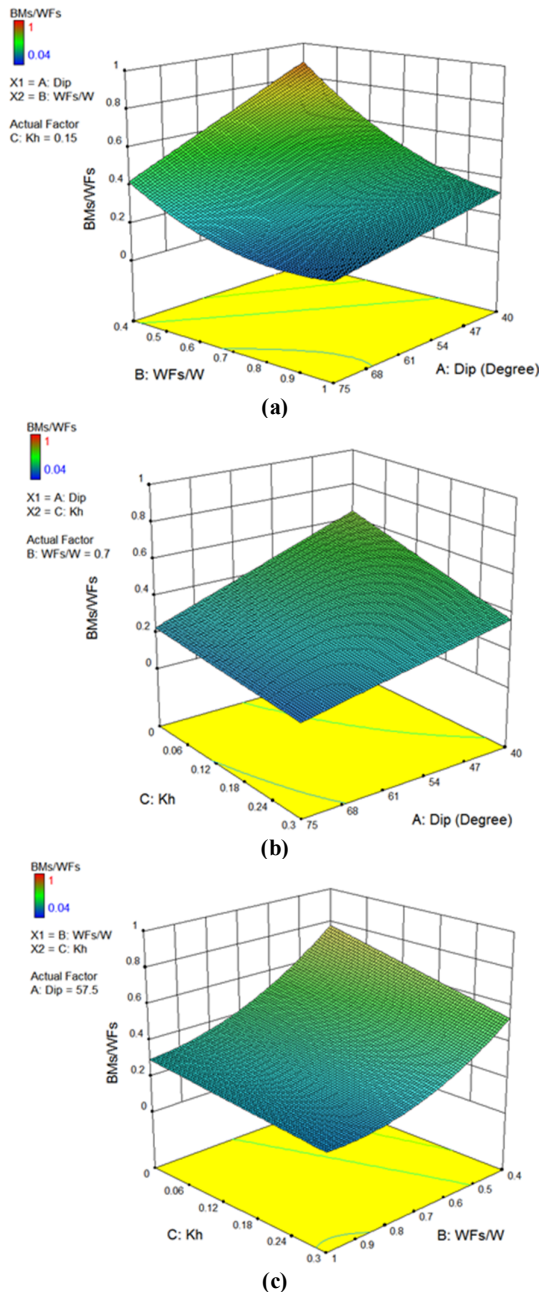
(a)

(b)

(c)

Figure 12. Effects of the dip angle and normalized free span interaction (a), dip angle and horizontal acceleration coefficient interaction (b), and normalized free span and horizontal acceleration coefficient interaction (c) in the 3D space on the maximum undercut span.

4. Conclusions

A series of 120 numerical simulations were conducted using FLAC 3D, as the finite difference software, under the static and pseudo-static conditions. The numerical results obtained were investigated with a statistical method using the response surface methodology (RSM). Then a non-linear relationship was interpolated between three input variables and one response. The influences of each input variable, both individual and simultaneous, on the response were studied using an analysis of variance (ANOVA). The results obtained illustrated that the influence of the counterweight on the stabilization of undercut slopes decreased as the slope angle increased. In steep slopes, the counterweight was seen to have almost no influence on the stabilization under either the static or the pseudo-static conditions. Thus the use of a counterweight can be considered as a beneficial method for increasing the stability of the mild undercut slopes such as those in surface coal mining. With a constant value for the normalized free span, as the horizontal acceleration coefficient increased, the maximum normalized undercut span decreased slightly but the rate of this decrease in a maximum normalized undercut span was greater at lower values for the normalized free span. A relationship was proposed for estimating the maximum normalized stable undercut span in terms of the slope angle, horizontal acceleration coefficient, and normalized free span of the slope.

References

[1]. Handy, R.L. (1985). The Arch in Soil Arching, J. Geotech. Eng., 111 (3): 302–318

[2]. Janssen, H.A. (1895). Versuche uber getreidedruck in Silozellen, Zeitschrift des Vereins Dtsch. Ingenieure, 35:1045–1049.

[3]. Terzaghi, K. (1943). Theoretical soil mechanics. John Wiley & Sons, New York., Theor. soil Mech. John Wiley Sons, New York.

[4]. Wang, W.L. and Yen, B.C. (1974). Soil arching in slopes, J. Geotech. Eng.

[5]. Bosscher, P.J. and Gray, D.H. (1986). Soil Arching in Sandy Slopes, J. Geotech. Eng., 112 (6): 626–645.

[6]. Pipatpongsa, T., Khosravi, M.H., and Takemura, J. (2013). Physical modeling of arch action in undercut slopes with actual engineering practice to Mae Moh open-pit mine of Thailand, in Proceedings of the 18th International Conference on Soil Mechanics and Geotechnical Engineering (ICSMGE18), 1: 943–946.

[7]. Zhou, J., Qin, C., Pan, Q., and Wang, C. (2019). Kinematic analysis of geosynthetics-reinforced steep slopes with curved sloping surfaces and under earthquake regions, J. Cent. South Univ., 26 (7): 1755–1768.

[8]. Zhang, R., Long, M., Lan, T., Zheng, J., and Geoff, C. (2020). Stability analysis method of geogrid reinforced expansive soil slopes and its engineering

application, J. Cent. South Univ., 27 (7): 1965–1980.

[9]. Hedayat, A., Haeri, H., Hinton, J., Masoumi, H., and Spagnoli, G. (2018). Geophysical signatures of shear-induced damage and frictional processes on rock joints, J. Geophys. Res. Solid Earth, 123 (2): 1143-1160.

[10]. Sarfarazi, V., Haeri, H., and Khaloo, A. (2016). The effect of non-persistent joints on sliding direction of rock slopes, Comput. Concr., 17 (6): 723–737.

[11]. Sun, S.W., Zhu, B.Z., and Wang, J.C. (2013). Design method for stabilization of earth slopes with micropiles, Soils Found., 53 (4): 487–497.

[12]. Chen, C.Y. and Martin, G.R. (2002). Soil-Structure interaction for landslide stabilizing piles, Comput. Geotech., 29 (5): 363–386.

[13]. Hosseinian, S. and Seifabad, M.C. (2013). Optimization the Distance between Piles in Supporting Structure Using Soil Arching Effect, 3 (6): 386–391.

[14]. Li, C., Wu, J., Tang, H., Wang, J., Chen, F., and Liang, D. (2015). A novel optimal plane arrangement of stabilizing piles based on soil arching effect and stability limit for 3D colluvial landslides, Eng. Geol., 195: 236–247.

[15]. Ausilio, E., Conte, E., and Dente, G. (2001). Stability analysis of slopes reinforced with piles, Comput. Geotech., 28 (8): 591–611.

[16]. Kourkoulis, R., Gelagoti, F., Anastasopoulos, I., and Gazetas, G. (2011). Slope Stabilizing Piles and Pile-Groups: Parametric Study and Design Insights, J. Geotech. Geoenvironmental Eng., 137 (7): 663–677.

[17]. Kourkoulis, R., Gelagoti, F., Anastasopoulos, I., and Gazetas, G. (2011). Hybrid method for analysis and design of slope stabilizing piles, J. Geotech. Geoenvironmental Eng., 138 (1): 1–14.

[18]. Pipatpongsa, T., Khosravi, M.H., Doncommul, P., and Mavong, N. (2009). Excavation problems in Mae Moh lignite open-pit mine of Thailand, in Proceedings of Geo-Kanto2009, 12: 459–464.

[19]. Khosravi, M.H., Pipatpongsa, T., Takahashi, A., and Takemura, J. (2011). Arch action over an excavated pit on a stable scarp investigated by physical model tests, Soils Found., 51 (4): 723–735.

[20]. Khosravi, M.H., Takemura, J., Pipatpongsa, T., and Amini, M. (2016). In-flight excavation of slopes with potential failure planes, J. Geotech. Geoenvironmental Eng., 142 (5): 601-611.

[21]. Khosravi, M.H., Tang, L., Pipatpongsa, T., Takemura, J., and Doncommul, P. (2012). Performance of counterweight balance on stability of undercut slope evaluated by physical modeling, Int. J. Geotech. Eng., 6 (2): 193–205.

[22]. Sarfaraz, H., Khosravi, M.H., Pipatpongsa, T., and Bakhshandeh Amnieh, H. (2020). Application of Artificial Neural Network for Stability Analysis of Undercut Slopes, Int. J. Min. Geo-Engineering, In-press.

[23]. Terzaghi, K. (1950). Mechanism of landslides, Appl. Geol. to Eng. Pract. Geol. Soc., 83–123.

[24]. Khosravi, M.H., Sarfaraz, H., Esmailvandi, M., and Pipatpongsa, T. (2017). A Numerical Analysis on the Performance of Counterweight Balance on the Stability of Undercut Slopes, Int. J. Min. Geo-Engineering, 51 (1): 63–69.

[25]. Inc, I.G. (2015). FLAC3D: Fast Lagrangian Analysis of Continua in 3 Dimension.

[26]. Myer, R.H. and Montgomery, D.C. (2002). Response surface methodology: process and product optimization using designed experiment. Taylor & Francis.

[27]. Montgomery, D.C. (2017). Design and analysis of experiments. John wiley & sons.

[28]. Anderson, M.J. and Whitcomb P.J. (2004). Optimizing processes using response surface methods for design of experiments., CRC Pres.

تحلیل پایداری عددی شیروانی‌های تحت حفاری با استفاده از روش سطح پاسخ

حسن سرفراز۱، محمد حسین خسروی۱*و تیراپونگ پیپاتپونگسا۲

۱- دانشکده مهندسی معدن، پردیس دانشکده های فنی، دانشگاه تهران، تهران، ایران

۲- دپارتمان مدیریت شهری، دانشگاه کیوتو، کیوتو، ژاپن

چکیده:

یکی از مهم‌ترین پارامترها در طراحی شیروانی‌های تحت حفاری، تعیین حداکثر دهانه پایدار است که به عوامل مختلفی از قبیل مقاومت برشی خاک و خصوصیات هندسی شیروانی مربوط می‌شود. بر اساس پدیده قوس زدگی، با زیر برش در شیروانی، نیروی ناشی از وزن شیروانی به قسمت‌های مجاور ناحیه زیر برش منتقل می‌شود و منجر به افزایش پایداری شیروانی می‌شود. با این وجود، اگر قسمت‌های مجاور ناحیه زیر برش از مقاومت کافی برخوردار نباشند، این انتقال نیرو ممکن است منجر به شکست در این نواحی شود. استفاده از بار تعادلی در قسمت‌های مجاور شیروانی، یک روش مفید و مؤثر برای جلوگیری از شکست است و به پایداری شیروانی کمک می‌کند. از این رو، ناحیه زیر برش پایدار می‌تواند افزایش یابد. در این تحقیق، با ا استفاده از مدل‌سازی عددی، تعیین حداکثر عرض زیر برش در دو شرایط استاتیک و شبه استاتیک ارزیابی شده است. بدین منظور ۱۲۰ مدل عددی در مقادیر مختلف زاویه شیروانی، ضریب لرزه‌ای شتاب افقی و عرض بار تعادلی اجرا شده است. نتایج حاصل از مدل‌سازی عددی با استفاده از روش آماری سطح پاسخ مورد بررسی و ارزیابی قرار گرفت. آنالیز واریانس به‌منظور بررسی تأثیر هر متغیر ورودی بر روی پارامتر پاسخ انجام شده است. همچنین، یک رابطه آماری برای محاسبه حداکثر عرض زیر برش برحسب پارامترهای ورودی ارائه شده است.

کلمات کلیدی: شیروانی تحت حفاری، مدلسازی عددی، تحلیل شبه استاتیک، روش سطح پاسخ.